PAPER

Check for updates

ReaxFF molecular dynamics study of mechanochemical degradation of PFPE lubricants on DLC in heat-assisted magnetic recording†

Himanshu Shekhar, [ID] [a] Shota Uchiyama,[a] Yuxi Song,[a] Hedong Zhang, [ID] *[a] Kenji Fukuzawa,[b] Shintaro Itoh[b] and Naoki Azuma [ID] [b]

Understanding the degradation mechanisms of perfluoropolyether (PFPE) lubricants is critical for the reliability of Heat-Assisted Magnetic Recording (HAMR) systems. In this study, we conducted ReaxFF reactive molecular dynamics simulations to investigate the role of diamond-like carbon (DLC) surfaces in PFPE degradation under confined shear and at elevated temperature. The results show that confined shear plays a more dominant role than temperature, with the decomposition rate constant increasing with shear velocity. PFPE degradation primarily initiates through C–OH bond rupture at end groups, typically after the OH group bonds to the DLC surfaces. Bonded PFPE molecules adopt bridge and loop conformations, both contributing comparably to degradation with increasing shear velocity, with bridges being slightly more sensitive to shear. Our analysis suggests that bridge dissociation is facilitated by shear-induced end-to-end stretching, while loop dissociation is driven by entanglement of conformationally flexible main chains. These insights provide guidance regarding further development of reliable HAMR systems.

Introduction

The rapid expansion of Artificial Intelligence and big data analytics has driven the need for advancements in data storage technologies, particularly in increasing the areal density of hard disk drives (HDDs). In HDDs, data are stored within magnetic granular thin-film media, where individual grains serve as discrete recording units. Increasing areal density requires reducing the size of these grains to pack more data per unit area. However, shrinking grain size introduces thermal stability challenges, as smaller grains become prone to unintended magnetization reversals even at low temperatures. Heat-Assisted Magnetic Recording (HAMR) addresses this issue by employing high-anisotropy materials, such as $L1_0$-FePt, which enhance thermal stability. However, this increased anisotropy also leads to higher coercivity, making data writing difficult.[1] To mitigate this challenge, a near-field optical transducer, integrated within the write head in HAMR, focuses a laser beam onto a nanometer-scale region of the disk surface, momentarily heating it to 700–800 K.[2] This localized heating lowers the coercivity of the recording material, allowing a weaker magnetic field to effectively switch the magnetization of individual grains. Once the heat source is removed, the material rapidly cools back to room temperature, restoring its high coercivity and ensuring long-term data stability.

While HAMR effectively mitigates the challenges associated with smaller grain sizes, it introduces new concerns. The high temperatures required for writing, though applied for very short durations, can degrade the protective lubricant films on the disk surface. In HAMR systems, these films are typically composed of perfluoropolyether (PFPE), which protect both the head and disk from damage caused by their intermittent contacts during HDD operation.[3] The PFPE film is deposited at a thickness of 1–2 nm over the diamond-like carbon (DLC) overcoat of disk surfaces using a dip-coating technique.[4,5] During HDD operation, PFPE lubricants may undergo mechano-chemical,[6] thermal,[7,8] and catalytic degradation[9,10] depending on their working environment. Moreover, the combined effects of high temperatures and confined shear between the head and disk can significantly accelerate the decomposition of the lubricant films, resulting in further degradation.[6,11] This degradation can result in the formation of undesirable by-products and smear, ultimately compromising the reliability of the data read/write processes and reducing the operational lifespan of HDDs.[9] In HAMR systems, the normal pressure remains relatively constant (~0.2 GPa), but the shear velocity varies from 5–40 ms^{-1} depending on the inward or outward position of the head on the disk.[12,13] Therefore,

[a]*Department of Complex Systems Science, Graduate School of Informatics, Nagoya University, Furo-cho, Chikusa-ku, Nagoya 464-8601, Japan. E-mail: zhang@i.nagoya-u.ac.jp*

[b]*Department of Micro-Nano Mechanical Science and Engineering, Nagoya University, Furo-cho, Chikusa-ku, Nagoya 464-8603, Japan*

understanding the behavior and stability of PFPE lubricants under such extreme conditions is critical for advancing HAMR technology and ensuring its efficiency and reliability in high-density data storage applications.

Prior studies by Liu et al. investigated the thermal decomposition of PFPE lubricants, identifying reaction pathways for PFPE degradation and finding that cleavage of C–O bonds leads to the detachment of functional end groups and subsequent decomposition into smaller molecules.[8] However, beyond thermal effects, shear stress has been widely observed to accelerate reaction rates, leading to mechanochemical degradation. Several studies have reported an increase in reaction rates with sliding speed/shear rate across different systems. Harrington and Zimm demonstrated that hydrodynamic shear-driven polymer degradation follows first-order reaction kinetics, where shear stress facilitates polymer bond scission.[14] Similarly, shear stress has been shown to induce degradation in biomolecules[15] and lubricant additives,[16] further emphasizing its role in mechanochemical reactions. Zhang and Spikes demonstrated experimentally that shear stress significantly reduces the activation energy required for lubricant decomposition, confirming a stress-promoted thermal activation model for tribofilm formation.[17] Latorre et al. used ReaxFF-based[18,19] MD simulations to show that the dissociation rate of lubricant additives follows an exponential dependence on temperature and shear stress, further validating the importance of shear-induced degradation mechanisms.[20] More recently, Li et al. combined experimental and simulation approaches to investigate tribochemical reactions at sliding interfaces, demonstrating that shear stress influences tribofilm formation through mechanochemical activation.[21] These findings collectively underscore the critical influence of shear stress in lubricant degradation and motivate the need to further explore its role in confined PFPE degradation on DLC surfaces.

Within HAMR systems, Chen et al. demonstrated that PFPE degradation can be driven by elevated contact pressure as well as the catalytic effects of water.[6,9] Beyond operating conditions, the DLC overcoat itself plays a crucial role in PFPE degradation. The interaction between lubricants and DLC has been extensively studied, with experimental research exploring the degradation and behavior of PFPE on DLC coatings.[22–25] Zhao and Bhushan demonstrated that PFPE decomposes into small molecular fragments due to C–O bond rupture in the end groups of lubricant molecules, driven by triboelectric reactions and mechanical scission. This degradation ultimately results in DLC wear, further compromising HDD longevity.[22,23] They also observed experimentally that the partial pressure of PFPE fragments generated during decomposition over DLC increased rapidly with sliding velocity.[23] Lee et al. found that particle generation rates increased at higher shear speeds, attributing this to slider–disk interactions.[24] Their surface analysis revealed that these particles contained lubricant remnants, disk coating layers, and material from the slider surface.

In addition to experimental studies, reactive molecular dynamics (MD) simulations have provided further insights into DLC-induced lubricant degradation. Using ReaxFF-based[18,19] MD simulations, Lotfi et al. concluded that the presence of DLC significantly enhances PFPE decomposition, particularly at elevated temperatures.[25] While previous studies have explored thermal and shear-induced degradation of PFPE, these investigations used hydrogen-passivated diamond surfaces rather than DLC.[6,9] Therefore, the combined effects of confined shear, PFPE–DLC interactions, and high temperatures—conditions inherent to HAMR operation—remain unexplored. These factors may introduce complex mechanochemical effects. Further research is needed to elucidate these mechanisms and their implications for lubricant stability in HAMR-based HDDs.

In this study, we employ non-equilibrium reactive MD simulations to gain molecular-level insights into the degradation of PFPE lubricant molecules subjected to confined shear by DLC surfaces under HAMR operating conditions. By varying shear velocity and temperature, we compare reaction rates to assess the relative significance of each parameter. To investigate the specific mechanisms driving PFPE degradation, we identify the primary bond dissociation that initiates lubricant decomposition and key factors leading to bond breakage. The insights from this study are critical for understanding the fundamental processes governing lubricant degradation and for developing strategies to mitigate these effects, thereby enhancing the reliability and efficiency of HAMR systems.

Materials and methods

The lubricant used in this study was PFPE D-4OH, similar to those employed in the head–disk interface (HDI). The chemical formula of D-4OH, which consists of a main chain (MC) and two end groups (EGs),[9] is shown in Fig. 1, and its molecular weight is 1820 g mol^{-1}. The head and disk were modeled as DLC surfaces on diamond substrates, as shown in Fig. 2. The head was represented as a slab instead of a curved surface, as its practical curvature radius ($\sim$20 mm) far exceeds the lateral dimensions of the contact region.[9,12] These DLC surfaces were formed by argon bombardment of the diamond substrates[26] at 3500 K, achieving an sp^2 carbon ratio of approximately 20% consistent with the structure employed in a previous tribological study.[27] A pre-validated ReaxFF[18,19] force field (by Chen et al.[6]) was employed to model interactions between constituent atoms.

A total of 40 D-4OH molecules were confined between the head and disk, both with dimensions of 8.04624 nm $\times$ 8.04624 nm in the x and y directions. Periodic boundary conditions were applied in all three directions. To prevent interactions with image cells in the z direction, 2 nm thick vacuum layers were added above the head and below the disk. The following preparation procedures were conducted

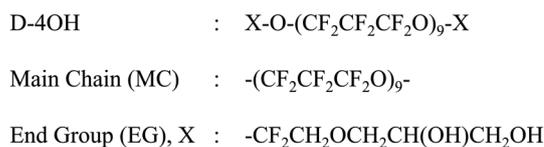| D-4OH	:	X-O-(CF$_2$CF$_2$CF$_2$O)$_9$-X
Main Chain (MC)	:	-(CF$_2$CF$_2$CF$_2$O)$_9$-
End Group (EG), X	:	-CF$_2$CH$_2$OCH$_2$CH(OH)CH$_2$OH

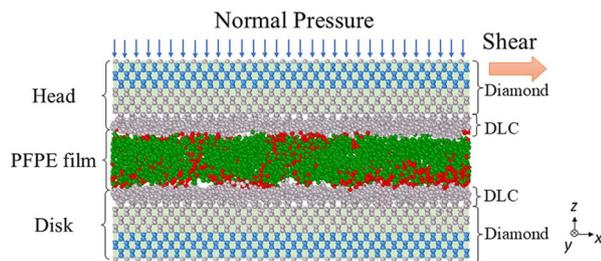Fig. 1 Chemical formula of D-4OH, consisting of a Main Chain (MC) and two End Groups (EGs).

Fig. 2 Initial configuration of the shear simulation model after compression, showing the lubricant film confined between the head and disk. The head and disk are composed of a DLC layer over diamond. Dark green and red represent the atoms of the MC and EGs of D-4OH, respectively. Atoms coupled with a thermostat are represented in blue inside the head and disk.

according to the methodology outlined by Chen *et al.*[9] To minimize the degradation of D-4OH molecules during system preparation, a series of compression, relaxation, and recompression steps was performed. Initially, 40 D-4OH molecules were placed between two DLC surfaces, with fixed outermost carbon atoms on the lower surface. A normal pressure of 0.1 GPa was applied to the upper surface to compress the molecules and form a thin liquid film at 393 K. During this step, the non-reactive COMPASS II[28,29] force field was employed to avoid any unintended bond dissociation. Following compression, the system was relaxed by lifting the upper substrate and holding the temperature at 393 K for 1 ns, followed by a further 1 ns relaxation at 293 K. The force field was then switched from COMPASS II[28,29] to ReaxFF[18,19] to enable reactive MD simulations. To minimize atomic displacements and avoid artifact bond ruptures due to differences in equilibrium configurations between the two force fields, the temperature was reduced to 1 K for 1 ps. Subsequently, the system was heated to 293 K at a controlled rate of 292 K ps^{-1}. A direct compression under constant pressure was avoided, as it could result in high-velocity impacts from the upper DLC surface, potentially triggering unintended degradation. As an alternative, we initially conducted a separate set of simulations to determine the equilibrium interfacial separation corresponding to the target normal pressure. Final film formation was performed using a two-step compression protocol to reach the identified equilibrium gap. First, a normal pressure of 0.1 MPa was applied to the upper substrate for 50 ps. This was followed by a constant-velocity compression at 20 ms^{-1} in the negative z-direction for 30 ps. Finally, the system was gradually heated from 293 to 700 K over 40 ps to replicate operating conditions of HAMR. A timestep of 1.0 fs was used for the COMPASS II[28,29] simulations, 0.1 fs during the force field switch, and 0.2 fs for the ReaxFF[18,19] equilibration. The final equilibrated structure, shown in Fig. 2, was then used as the starting configuration for shear simulations.

In the shear simulations, a constant velocity in the x-direction and a constant normal pressure in the negative z-direction were applied to the uppermost layer of atoms on the head. The disk was constrained by fixing the lowermost layer of atoms.

The Langevin thermostat[30] with a damping coefficient of 10 fs was applied exclusively to the intermediate layers of the head and disk (marked in blue in Fig. 2) to prevent unphysical behavior in the lubricant molecules.[31] The thermostat was applied only in the *y*-direction—perpendicular to the directions of applied forces (x and z)—to regulate system temperature without directly influencing the mechanical response to shear and normal stresses. As shown in Fig. S1 of the ESI,† the net shear force—given by the sum of shear stresses on the upper and lower surfaces—remains balanced around zero. Additionally, Fig. S2† shows that the temperature remained close to the target value throughout the simulation.

To study the effect of temperature, simulations were conducted at target temperatures of 293 and 700 K at a normal pressure of 0.2 GPa and shear velocity of 25 ms^{-1}. To examine the effect of confined shear on lubricant degradation, simulations were conducted at shear velocities of 0, 5, 10, 15, 20, and 25 ms^{-1} at a normal pressure of 0.2 GPa and a temperature of 700 K. Ten independent simulations were performed for each case using different initial configurations. All simulations were run for 0.5 ns with a timestep of 0.2 fs, and reaction rates were analyzed over the entire shear simulation period.

All MD simulations were executed using LAMMPS (Large-Scale Atomic/Molecular Massively Parallel Simulator).[32,33] Initial configurations were prepared using packmol[34] and moltemplate,[35] and the simulation results were visualized using OVITO.[36]

Results and discussion

The study investigated the reaction rates during shear simulations of D-4OH molecules by DLC surfaces. The reaction rate constant (k) was determined by fitting the following equation assuming first-order reaction kinetics:[37]

$$\ln(N_t/N_0) = -kt \qquad (1)$$

where N_t and N_0 represent the number of intact D-4OH molecules at time t and at the initial time $t = 0$, respectively. Fig. 3 illustrates the temporal evolution of $\ln(N_t/N_0)$ for D-4OH on DLC surfaces under simulation conditions of 700 K, 0.2 GPa normal pressure, and 25 ms^{-1} shear velocity. The result is fitted by a straight line represented by eqn (1). The reaction rate constant k was determined to be 5.3×10^9 s^{-1} on DLC. This value is significantly higher than that for hydrogen-passivated diamond surfaces, where no reactions were observed under identical simulation conditions, as previously reported by Chen *et al.*[9] This shows that the presence of DLC significantly accelerates the degradation of D-4OH.

The reaction rate on DLC can be affected by factors such as temperature and confined shear. To investigate these influences, two simulation setups were designed: one with the head present and one without. In the former, the head was subjected to a normal pressure of 0.2 GPa and a shear velocity of 25 ms^{-1}, enabling the study of the effect of confined shear on k in comparison to the latter unconfined case. Both setups were evaluated at two temperatures, 293 and 700 K, to assess the
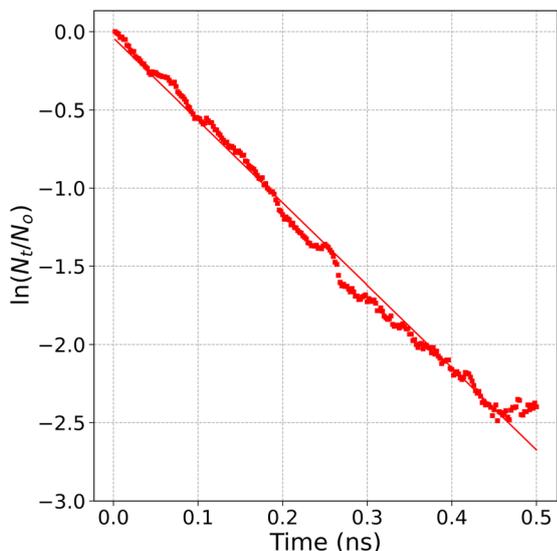
Fig. 3 Temporal evolution of $\ln(N_t/N_0)$ for unreacted D-4OH molecules under confined shear by DLC surfaces, averaged over 10 simulations at 0.2 GPa normal pressure and 700 K.

Fig. 5 Reaction rate constants k at varying shear velocities under fixed conditions of 700 K and 0.2 GPa normal pressure. Error bars represent the standard deviation across 10 simulations.

influence of temperature under each condition. The k value was determined for each case following eqn (1).

Fig. 4 illustrates the k values for both setups, with error bars representing the standard deviation across 10 simulations. The results confirm that k increases with temperature, as the values at 700 K are higher than those at 293 K in both setups. The k value at 293 K without confinement is significantly lower than in all other cases, nearly zero, confirming the stability of D-4OH at room temperature. This also indicates that either confined shear or high temperature is necessary for decomposition of D-4OH on DLC. Furthermore, the k values under confined shear
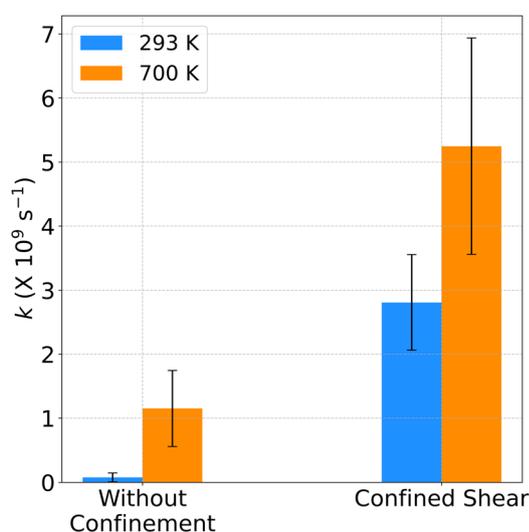
are higher than those without confinement at the same temperature. Notably, the k value observed under confined shear at 293 K is approximately three times that recorded without confinement at 700 K. These findings demonstrate that confined shear plays a dominant role in the decomposition of D-4OH, surpassing the influence of temperature.

Consequently, we investigated the impact of confined shear, focusing specifically on the influence of shear velocity.

Fig. 4 Comparison of reaction rate constants (k) at two temperatures (293 and 700 K) under conditions without confinement and with confined shear. For the former condition, the head was absent, and D-4OH degradation was driven solely by temperature. Error bars represent the standard deviation across 10 simulations.
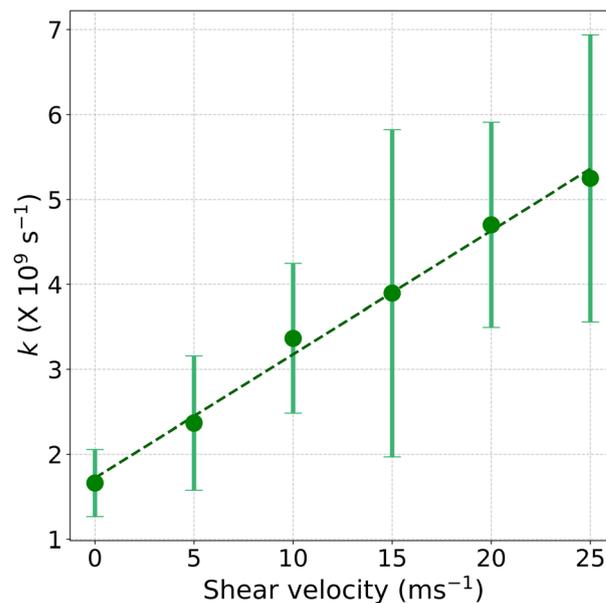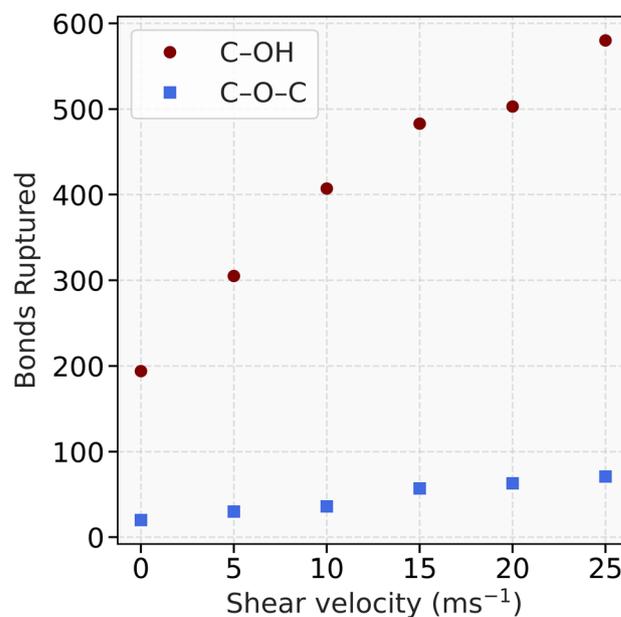

Fig. 6 Total number of C−OH and C−O−C bonds ruptured at various shear velocities. The data represent the cumulative results from 10 simulations.
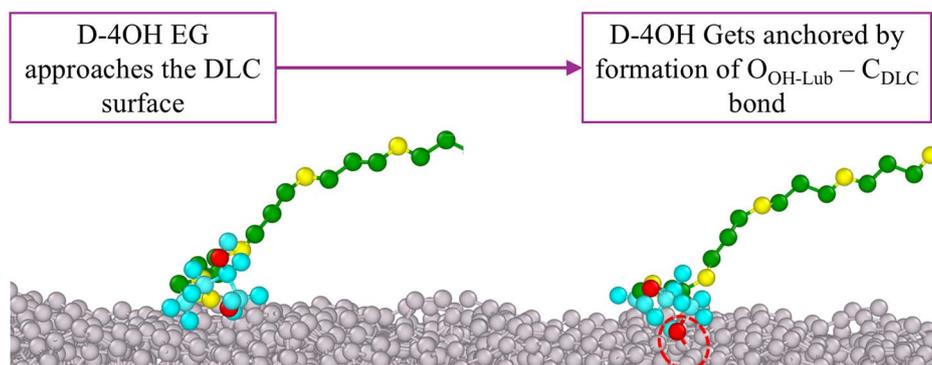
Simulations were conducted at shear velocities ranging from 0–25 ms^{-1}, maintaining a temperature of 700 K and a normal pressure of 0.2 GPa as these conditions closely replicate the operating conditions of HAMR systems.[2,12,13] Fig. 5 illustrates the relationship between k and shear velocity. The observed k values increase linearly from approximately 1.6×10^9 to 5.5×10^9 s^{-1}, with the lowest value corresponding to 0 ms^{-1}, which can be attributed solely to confinement under normal pressure. This increase in k is consistent with experimental observations, where higher sliding velocities correlated with an increased formation of degradation byproducts.[23,24] Additionally, in line with previous studies,[38,39] the shear stress averaged over the 0.5 ns shear simulations increases approximately logarithmically with shear velocity (Fig. S3 in the ESI†). The rise in the reaction rate constant is likely driven by the corresponding increase in shear stress.[17,20,21]

To gain further insights into the D-4OH degradation mechanisms, we quantified the first bond dissociation event as a representative indicator of molecular decomposition. The analysis shows that most degradation events resulted from the rupture of C–OH and C–O–C bonds of D-4OH molecules (Fig. 1). Additionally, a small fraction of bond ruptures involved C–O–C

bonds within the MC. These findings align with previous studies, which reported that the degradation of PFPE molecules predominantly involves the cleavage of C–O bonds[6,9,40] and the EGs are the primary sites of PFPE decomposition.[41,42] Consequently, we counted the number of C–OH and C–O–C bond dissociations marking the first bond rupture in any D-4OH molecule across 10 independent simulations over the 0.5 ns runtime, encompassing a total of 400 molecules. Fig. 6 depicts the total number of first-ruptured C–OH and C–O–C bonds at various shear velocities. The number of first-ruptured C–OH bonds ranged from approximately 200 to 600 across shear velocities of 0–25 ms^{-1}—substantially higher than the corresponding C–O–C bond ruptures observed over the same velocity range. This indicates that C–OH bonds are more vulnerable to confined shear than C–O–C bonds, making C–OH bond rupture the primary pathway for the initial degradation of D-4OH.

To elucidate the mechanisms of C–OH bond rupture, we analyzed the associated reaction pathways. Fig. 7 illustrates that the reaction proceeds in two phases. In the first phase (Fig. 7a), a hydroxyl group from the EGs of a D-4OH molecule approaches the DLC surface, where the hydroxyl oxygen attaches to the sp^2 hybridized carbon atom of the DLC surface, causing O$_{OH-Lub}$–
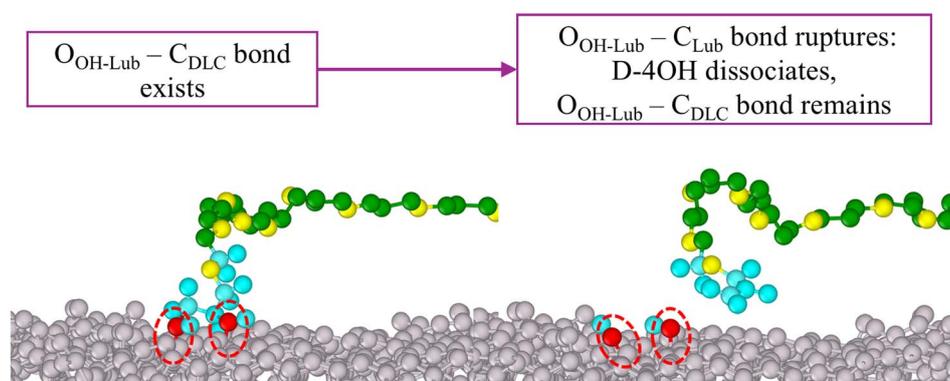

Fig. 7 Snapshots illustrating the two-phase reaction pathway for the initial decomposition of D-4OH on DLC: (a) O$_{OH-Lub}$–C$_{DLC}$ association (OCA) and (b) O$_{OH-Lub}$–C$_{Lub}$ dissociation (OCD). Hydroxyl oxygen atoms are depicted in red, while the remaining EG atoms are shown in sky blue. Oxygen atoms other than hydroxyl oxygen are colored yellow, and carbon atoms of the MC are represented in green. Fluorine atoms have been omitted for clarity.

C_{DLC} association (OCA). Any EG within the D-4OH molecule can participate in this reaction. In the second phase (Fig. 7b), the D-4OH molecule decomposes *via* the C–OH bond cleavage in the EGs of the molecule, corresponding to O_{OH-Lub}–C_{Lub} dissociation (OCD). Notably, this C–OH bond rupture mostly occurs after bonding to DLC surfaces in the first phase, demonstrating that the reactivity of DLC surfaces plays a crucial role in the initial decomposition of D-4OH. Similar two-phase reactions between lubricant molecules and DLC surfaces have been reported in previous studies using the density-functional-based tight-binding method.[43,44] However, during the OCA process, this study showed that most hydroxyl groups remained intact, whereas previous studies reported that hydroxyl hydrogen first detaches, leaving an O radical that subsequently bonds to the sp^2 carbon of DLC surfaces. This discrepancy may stem from the limited accuracy of ReaxFF in capturing the deprotonation process. Nevertheless, the presence or absence of hydroxyl hydrogen should have minimal influence on the OCD reaction, because O_{OH-Lub}–C_{Lub} bond rupture is primarily driven by mechanical stretching, as will be discussed below, a finding that is also consistent with previous studies.[43–45]

As the majority of D-4OH molecules undergo decomposition through C–OH bond rupture following their adsorption onto DLC surfaces, we analysed the conformational states adopted by these molecules upon bonding. Bonded D-4OH molecules can adopt a tethered conformation, where only one EG is attached to the surface. Additionally, bonded D-4OH can also form two distinct conformations: bridges and loops. Bridges are formed when one EG group undergoes OCA on one DLC surface and the other EG on the opposing surface, as illustrated in Fig. 8 (left) and Movie 1 in the ESI.† Loops are formed when both EGs undergo OCA on the same DLC surface (either upper or lower), as shown in Fig. 8 (right) and Movie 2 in the ESI.† During simulations, both bridges and loops were observed to dissociate *via* OCD. Moreover, the mobile end of tethered molecules can diffuse to the opposing DLC surface to form bridges or the same DLC surface to form loops *via* OCA. This phenomenon is supported by previous studies, which indicate that as the head–disk gap approaches approximately 1 nm, lubricant molecules tend to diffuse toward the head surface.[46] Computational studies also suggest that PFPE molecules can diffuse to the upper substrate under the influence of pressure and temperature, even in the absence of lateral movement of the upper surface.[47,48]
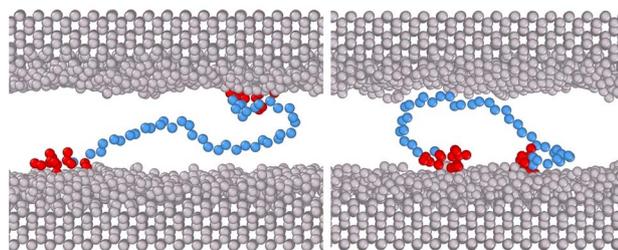

Fig. 8 Snapshots showing bridge (left) and loop (right) conformations of bonded D-4OH. The two DLC surfaces are shown in gray, the EG atoms are in red, and the MC atoms are in blue. Fluorine atoms are omitted for clarity.
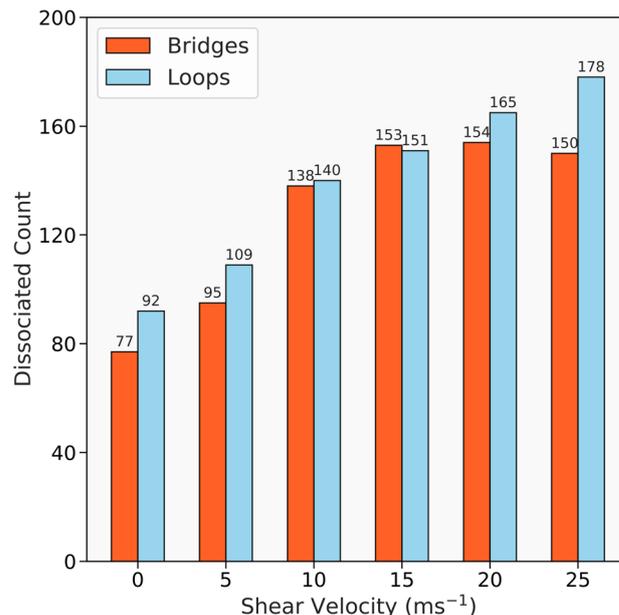

Fig. 9 Number of dissociated bridges and loops at various shear velocities. The data represent the cumulative results from 10 simulations.

To identify which conformation—bridges or loops—accounts for the majority of dissociated D-4OH molecules, we quantified the number of dissociated molecules in each category across different shear velocities, as shown in Fig. 9. It shows that the number of dissociated bridges and loops increases with shear velocity, particularly up to 15 ms^{-1}. Beyond this velocity, bridge dissociation plateaus, whereas loop dissociation continues to increase steadily. At each velocity, the number of dissociated bridges remains roughly comparable to that of loops, averaging only approximately 8% lower. These findings indicate that, despite the slightly different trends at higher shear velocities, both bridge and loop conformations contribute significantly to shear-induced degradation.

We further computed the probability of dissociation for each conformation, defined as the ratio of dissociated to formed conformations, in order to assess whether bridges or loops are more susceptible to shear-induced degradation. Fig. 10 presents the number of formed conformations, and Fig. 11 shows the probability of dissociation at various shear velocities. Similar to the trend in Fig. 9, Fig. 10 shows that the number of loops formed increases with shear velocity, whereas the number of bridges formed increases up to 10 ms^{-1} and then exhibits a slight decline. At lower velocities (≤15 ms^{-1}), bridges form in comparable or slightly higher numbers than loops, while at 20 and 25 ms^{-1}, more loops are formed than bridges. Averaged over all velocities, the number of formed bridges (160) is approximately 4% lower than that of loops (167). These trends in dissociation and formation (Fig. 9 and 10) are reflected in the dissociation probabilities shown in Fig. 11. Specifically, the dissociation probability of bridges is lower than that of loops up to 15 ms^{-1}, but this relationship reverses at higher velocities. Over the full range of 0 to 25 ms^{-1}, the dissociation probability
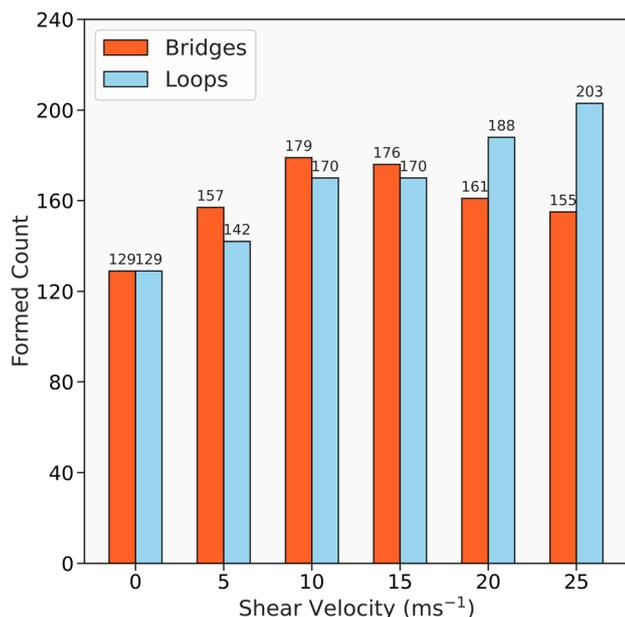
Fig. 10 Total number of bridges and loops formed at various shear velocities. The data represent the cumulative results from 10 simulations.
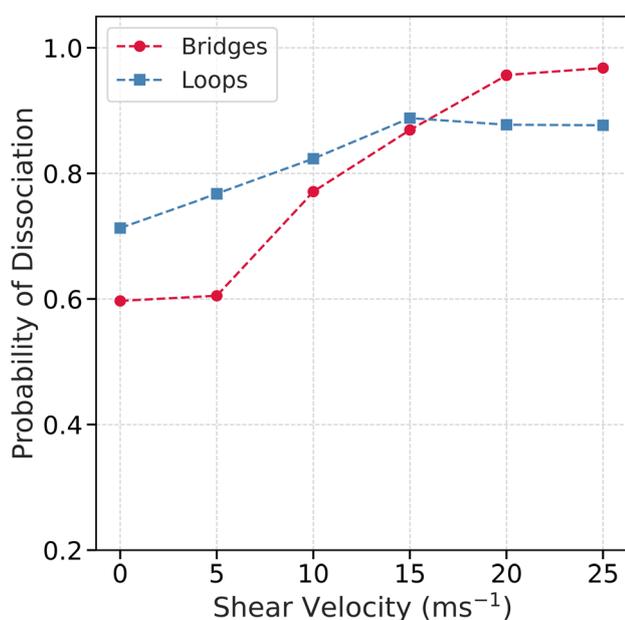

Fig. 11 Probability of dissociation of bridges and loops at various shear velocities.

increases from 0.60 to 0.97 for bridges and from 0.71 to 0.88 for loops, with the increase being more pronounced for bridges. This indicates that bridge dissociation is more sensitive to shear velocity than loop dissociation.

To understand why the dissociation probability of bridges and loops increases with shear velocity, we analysed the end-to-end distances (R_{ee}) of dissociated bridges and loops at the time of dissociation. Fig. 12 shows the results for dissociated bridges.
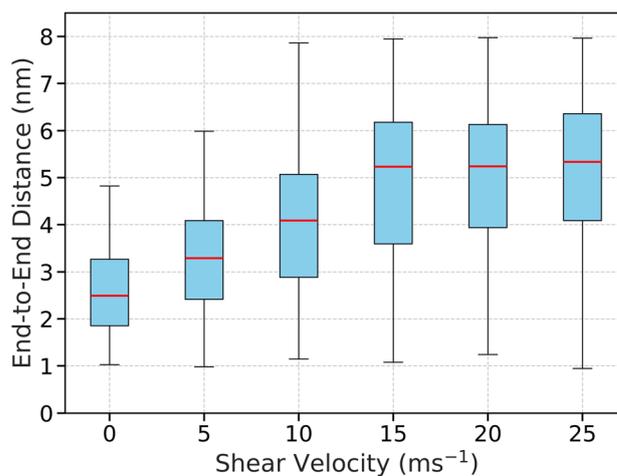

Fig. 12 Range of end-to-end distances (R_{ee}) at various shear velocities for all dissociated bridges. The red line within each box represents the median R_{ee} value, while the blue boxes indicate the interquartile range (25th–75th percentile). The whiskers extend to the minimum and maximum values.

While the minimum R_{ee} remains nearly constant across all shear velocities, the maximum, median, and first quartile (Q1) R_{ee} values increase with velocity and plateau at 10, 15, and 20 ms^{-1}, respectively. These trends indicate that bridges tend to be more extended at higher shear velocities. Notably, at 20 and 25 ms^{-1}, approximately 75% of dissociated bridges exhibit R_{ee} values greater than 4 nm (half the observed maximum R_{ee}). This increasing proportion of extended bridges aligns with the elevated dissociation probabilities observed in Fig. 11, suggesting that molecular extension contributes to the likelihood of dissociation. Supporting this, Movie 1 (ESI†) visually demonstrates the progressive extension and rupture of a bridge-forming D-4OH molecule under shear. As the shear velocity increases, bridges experience faster elongation, allowing them to reach higher R_{ee} values within shorter timeframes. However, Fig. 12 also reveals that bridge dissociation occur across a wide distribution of R_{ee}, including as low as 1 nm. This indicates that complete extension is not a necessary condition for bridge dissociation *via* OCD. Dissociation events at such low R_{ee} values are attributed to local mechanical constraints imposed by neighboring molecules, which restrict molecular mobility and concentrate tensile stress on specific bonds, particularly at the adsorbed EGs.

Taken together, these findings suggest that molecular extension contributes to—but does not solely determine—the dissociation of bridges. While bridges with higher R_{ee} are statistically more likely to dissociate, the underlying cause is not elongation alone, but rather the cumulative effect of dynamic local stress distributions that arise more frequently under shear. Thus, the consistent criterion for degradation remains the rupture of the C–OH bond, triggered by dynamically evolving local stress conditions rather than a uniform critical extension threshold.

Fig. 13 presents the R_{ee} values of dissociated loops at different shear velocities. In contrast to dissociated bridges,
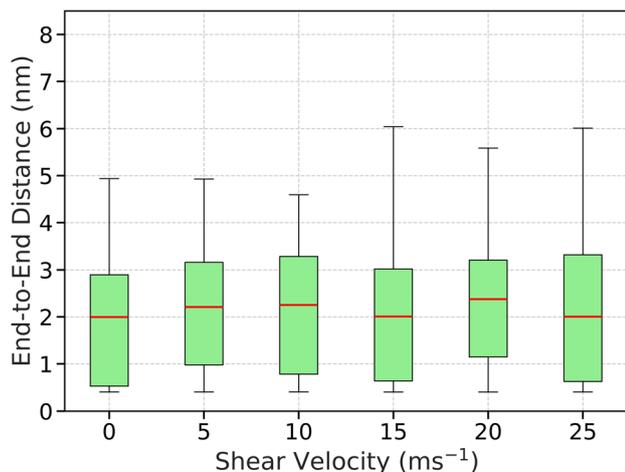
Fig. 13 Range of end-to-end distances (R_{ee}) at various shear velocities for all dissociated loops. The red line within each box represents the median R_{ee} value, while the green boxes indicate the interquartile range (25th–75th percentile). The whiskers extend to the minimum and maximum values.

loops exhibit relatively stable R_{ee} distributions across all velocities, with the median, first quartile (Q1), and third quartile (Q3) values consistently around 2, 0.5, and 3 nm, respectively. This is expected, as both ends of a loop are anchored to the same DLC surface and therefore cannot undergo end-to-end elongation during shear. The most interesting observation from Fig. 13 is

that 75% of the dissociated loops have R_{ee} values below 3 nm, which is significantly shorter than the molecule's maximum extension length (around 8 nm). This indicates that loops with smaller R_{ee} are more susceptible to dissociation than those with larger R_{ee}. Loops with larger R_{ee} are likely to adopt a more extended conformation and lie flat on the surface, minimizing interference with other molecules. Conversely, loops with smaller R_{ee} have more conformational freedom in their MCs, increasing the likelihood of entanglement with surrounding molecules. Consequently, unlike bridge dissociation, which is primarily driven by direct end-to-end stretching, loop degradation arises from alternative mechanisms involving localized stress on the EGs, induced by the entanglement of conformationally flexible MCs.

This loop dissociation mechanism can be better understood through Fig. 14 and Movie 2 (ESI†), where two entangled loops were randomly selected to demonstrate a dissociation event. The two loop-forming D-4OH molecules are both anchored to the same DLC surface and located in close spatial proximity. One molecule (Mol I), with a green MC, is oriented at an angle to the x-direction and obstructs the shear-driven motion of a neighbouring molecule (Mol II), which has a maroon MC. This obstruction builds up localized tensile stress in Mol I, ultimately leading to C–OH bond rupture.

Fig. 11 shows that shear velocity increases the probability of loop dissociation, although at a more modest rate than for bridges. This trend suggests that localized stress events become more frequent under high-velocity shear. A plausible
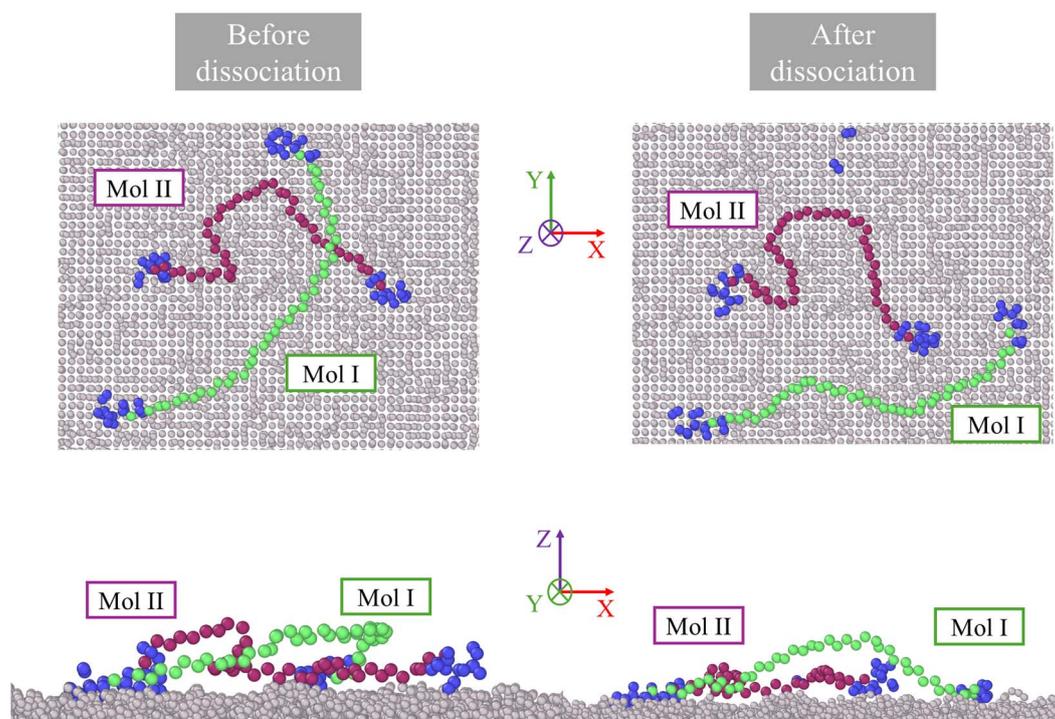
Fig. 14 Top view (above) and side view (below) of two loops formed on the lower DLC surface before and after dissociation. Two molecules of D-4OH form loops on the lower surface. Mol I (green MC) overlaps Mol II (maroon MC). Shear velocity is applied in the x-direction through the movement of the upper substrate (not shown for clarity). EG atoms are shown in blue. Other lubricant molecules and fluorine atoms have been omitted for clarity.

explanation is that, at higher shear velocities, a greater proportion of bridges become extended, increasing the likelihood of entanglement between loop MCs and these stretched bridges. The mechanical stress in the extended bridges may then be transferred to loops—particularly at their adsorbed EGs—thereby promoting bond rupture.

Since bridges will eventually rupture under continuous shear, and loops with smaller R_{ee} are also prone to dissociation, suppressing the formation of both bridges and loops with conformationally flexible MCs emerges as a key strategy for mitigating lubricant degradation under confined shear in HAMR systems. One approach involves modifying the lubricant architecture or disk overcoat material to enhance lubricant–disk interactions. This favours loop formation on the disk side and reduces the number of tethered chains, thereby lowering the likelihood of bridge formation. A representative example is the use of multidentate lubricants, such as ZTMD and 24TMD, which have demonstrated improved durability due to their flatter molecular conformation on the disk surface. These conformations reduce the likelihood of formation of bridges or loops with conformationally flexible MCs.[49,50] A second approach involves modifying the head overcoat material to minimize its affinity for lubricant functional groups. This would further suppress bridge formation and, in turn, minimize lubricant molecular dissociation. Together, these approaches warrant further exploration to improve the reliability and performance of HAMR systems.

Conclusion

We conducted ReaxFF reactive MD simulations to investigate the role of DLC surfaces in the degradation of PFPE D-4OH lubricant films under confined shear and at elevated temperatures during HAMR operations. The results reveal that DLC significantly accelerates the degradation of D-4OH, in contrast to hydrogen-passivated diamond surfaces where degradation was not observed under identical conditions. Comparing cases with and without confined shear at different temperatures, we found that confined shear plays a dominant role in D-4OH dissociation, surpassing the influence of temperature. Notably, the decomposition rate constant increases linearly with shear velocity, emphasizing the critical role of shear-induced mechanochemical effects.

The D-4OH decomposition was found to primarily begin with C–OH and C–O–C bond ruptures, with C–OH bond cleavage being the dominant pathway. Our analysis confirms that most C–OH bond ruptures occur *via* a two-step process: the hydroxyl oxygen of D-4OH first bonds to the DLC surfaces, followed by bond cleavage, highlighting the reactivity of DLC in facilitating decomposition. Upon bonding to DLC, D-4OH molecules predominantly adopted two conformations—loops and bridges. Both conformations contribute comparably to degradation with increasing shear velocity, with bridges exhibiting slightly greater sensitivity to shear. Analysis of R_{ee} distributions for dissociated bridges and loops reveals that bridges with higher R_{ee} values are prone to dissociation, whereas loops show the opposite trend. The correlation between R_{ee}

distributions and dissociation probabilities suggests that bridge dissociation is facilitated by end-to-end stretching, while loop dissociation is driven by entanglement of conformationally flexible MCs.

These findings provide mechanistic insights into shear-driven lubricant degradation at the HDI, highlighting the importance of DLC interactions and molecular conformation. Such insights are crucial for developing more stable PFPE lubricants, ultimately enhancing the efficiency and longevity of HAMR systems and advancing high-density data storage technologies.

Future work could involve the application of the Bell model to calculate activation energies and activation volumes associated with D-4OH dissociation. Such an approach would provide further quantitative insight into how mechanical stress lowers energy barriers for bond rupture, further advancing the mechanochemical interpretation of PFPE degradation.

Data availability

Due to the extensive volume of data generated in this study it is not possible to upload all simulation output files to a public repository. However, to maintain transparency, we have provided numerical data directly within the figures and text where relevant. Reaction rate constants (k) are explicitly reported in the text where necessary. The number of dissociated bridges and loops is shown in Fig. 9, while Fig. 10 presents the total number of formed bridges and loops at each shear velocity. Numeric values for each case are displayed over the corresponding bars in the bar graphs for clarity. These datasets form the foundation of our key conclusions and are made available within the manuscript.

Conflicts of interest

There are no conflicts to declare.

Acknowledgements

Notes and references

1 W.-H. Hsu and R. H. Victora, Heat-assisted magnetic recording — Micromagnetic modeling of recording media and areal density: a review, *J. Magn. Magn. Mater.*, 2022, **563**, 169973.

2 L. Huang, B. Stipe, M. Staffaroni, T. Hirano, E. Schreck and F. Y. Huang, in *2012 Digest APMRC*, 2012, pp. 1–2.

3 G. W. Tyndall, P. B. Leezenberg, R. J. Waltman and J. Castenada, Interfacial interactions of perfluoropolyether lubricants with magnetic recording media, *Tribol. Lett.*, 1998, **4**, 103–108.

4 Q. Liu, Y. Hu, X. Zhu, L. Peng, Z. Wang, K. Huang, Z. Chen, W. Wu and Y. Zhang, Nanoindentation-induced interface behavior between DLC film and monocrystalline silicon substrate at high temperature: a molecular dynamics simulation study, *Mater. Today Commun.*, 2024, **38**, 108205.

5 P. H. Kasai and C. Spiese, Interaction Between Disk Lubricants and Solvents in the Dip-Coating Process, *Tribol. Lett.*, 2004, **17**, 823–833.

6 X. Chen, K. Kawai, H. Zhang, K. Fukuzawa, N. Koga, S. Itoh and N. Azuma, ReaxFF Reactive Molecular Dynamics Simulations of Mechano-Chemical Decomposition of Perfluoropolyether Lubricants in Heat-Assisted Magnetic Recording, *J. Phys. Chem. C*, 2020, **124**, 22496–22505.

7 R. Ji, B. Xu, R. Zheng, H. Xie and J. W. H. Tsai, The Investigation of High Temperature Lubricants for HAMR Application, *IEEE Trans. Magn.*, 2013, **49**, 2772–2775.

8 Q. Liu, K. Huang, X. Zhu and G. Wang, Study on the Thermal Decomposition of D-4OH PFPE Lubricant by Reactive Molecular Dynamic Simulation for HAMR, *IEEE Trans. Magn.*, 2023, **59**, 1–7.

9 X. Chen, K. Inayoshi, H. Zhang, N. Koga, K. Fukuzawa, S. Itoh and N. Azuma, Effect of water on mechano-chemical reactions of perfluoropolyether lubricant films in heat-assisted magnetic recording: a reactive molecular dynamics study, *Tribol. Int.*, 2023, **187**, 108674.

10 P. H. Kasai and P. Wheeler, Degradation of perfluoropolyethers catalyzed by aluminum chloride, *Appl. Surf. Sci.*, 1991, **52**, 91–106.

11 Q. Cheng and D. B. Bogy, Experimental study of smear formation and removal in heat-assisted magnetic recording, *Tribol. Int.*, 2022, **165**, 107258.

12 S. Rajauria, O. Ruiz, S. V. Canchi, E. Schreck and Q. Dai, Electrostatically Tunable Adhesion in a High Speed Sliding Interface, *Phys. Rev. Lett.*, 2018, **120**, 026101.

13 Q. Cheng, PhD thesis, UC Berkeley, 2021.

14 R. E. Harrington and B. H. Zimm, Degradation of Polymers by Controlled Hydrodynamic Shear1, *J. Phys. Chem.*, 1965, **69**, 161–175.

15 T. A. Hakala, E. V. Yates, P. K. Challa, Z. Toprakcioglu, K. Nadendla, D. Matak-Vinkovic, C. M. Dobson, R. Martínez, F. Corzana, T. P. J. Knowles and G. J. L. Bernardes, Accelerating Reaction Rates of Biomolecules by Using Shear Stress in Artificial Capillary Systems, *J. Am. Chem. Soc.*, 2021, **143**, 16401–16410.

16 Y. Shimizu and H. A. Spikes, The Influence of Slide–Roll Ratio on ZDDP Tribofilm Formation, *Tribol. Lett.*, 2016, **64**, 19.

17 J. Zhang and H. Spikes, On the Mechanism of ZDDP Antiwear Film Formation, *Tribol. Lett.*, 2016, **63**, 24.

18 A. C. T. van Duin, S. Dasgupta, F. Lorant and W. A. Goddard, ReaxFF: A Reactive Force Field for Hydrocarbons, *J. Phys. Chem. A*, 2001, **105**, 9396–9409.

19 K. Chenoweth, A. C. T. van Duin and W. A. Goddard, ReaxFF Reactive Force Field for Molecular Dynamics Simulations of Hydrocarbon Oxidation, *J. Phys. Chem. A*, 2008, **112**, 1040–1053.

20 C. Ayestarán Latorre, J. E. Remias, J. D. Moore, H. A. Spikes, D. Dini and J. P. Ewen, Mechanochemistry of phosphate esters confined between sliding iron surfaces, *Commun. Chem.*, 2021, **4**, 1–11.

21 Y.-S. Li, F. H. Bhuiyan, J. Lee, A. Martini and S. H. Kim, Elucidating tribochemical reaction mechanisms: insights into tribofilm formation from hydrocarbon adsorbates coupled with tribochemical substrate wear, *RSC Mechanochem.*, 2024, **1**, 328–341.

22 X. Zhao and B. Bhushan, Comparison studies on degradation mechanisms of perfluoropolyether lubricants and model lubricants, *Tribol. Lett.*, 2001, **9**, 187–197.

23 X. Zhao and B. Bhushan, Studies on degradation mechanisms of lubricants for magnetic thin-film rigid disks, *Proc. Inst. Mech. Eng., Part J*, 2001, **215**, 173–188.

24 D. Y. Lee, J. Hwang and G. N. Bae, Effect of disk rotational speed on contamination particles generated in a hard disk drive, *Microsyst. Technol.*, 2004, **10**, 103–108.

25 R. Lotfi, A. Jonayat, A. C. T. van Duin, M. M. Biswas and R. Hempstead, A Reactive Force Field Study on the Interaction of Lubricant with Diamond-Like Carbon Structures, *J. Phys. Chem. C*, 2016, **120**, 27443–27451.

26 M. Joe, M.-W. Moon and K.-R. Lee, Atomistic simulations of diamond-like carbon growth, *Thin Solid Films*, 2012, **521**, 239–244.

27 Y. Mabuchi, T. Higuchi and V. Weihnacht, Effect of sp2/sp3 bonding ratio and nitrogen content on friction properties of hydrogen-free DLC coatings, *Tribol. Int.*, 2013, **62**, 130–140.

28 H. Sun, COMPASS: An *Ab Initio* Force-Field Optimized for Condensed-Phase ApplicationsOverview with Details on Alkane and Benzene Compounds, *J. Phys. Chem. B*, 1998, **102**, 7338–7364.

29 H. Sun, Z. Jin, C. Yang, R. L. C. Akkermans, S. H. Robertson, N. A. Spenley, S. Miller and S. M. Todd, COMPASS II: extended coverage for polymer and drug-like molecule databases, *J. Mol. Model.*, 2016, **22**, 47.

30 T. Schneider and E. Stoll, Molecular-dynamics study of a three-dimensional one-component model for distortive phase transitions, *Phys. Rev. B:Condens. Matter Mater. Phys.*, 1978, **17**, 1302–1322.

31 T. V. S. Krishnan, J. S. Babu and S. P. Sathian, A molecular dynamics study on the effect of thermostat selection on the physical behavior of water molecules inside single walled carbon nanotubes, *J. Mol. Liq.*, 2013, **188**, 42–48.

32 S. Plimpton, Fast Parallel Algorithms for Short-Range Molecular Dynamics, *J. Comput. Phys.*, 1995, **117**, 1–19.

33 A. P. Thompson, H. M. Aktulga, R. Berger, D. S. Bolintineanu, W. M. Brown, P. S. Crozier, P. J. in 't Veld, A. Kohlmeyer, S. G. Moore, T. D. Nguyen, R. Shan, M. J. Stevens, J. Tranchida, C. Trott and S. J. Plimpton, LAMMPS – a flexible simulation tool for particle-based materials modeling at the atomic, meso, and continuum scales, *Comput. Phys. Commun.*, 2022, **271**, 108171.

34 L. Martínez, R. Andrade, E. G. Birgin and J. M. Martínez, PACKMOL: a package for building initial configurations for molecular dynamics simulations, *J. Comput. Chem.*, 2009, **30**, 2157–2164.

35 A. I. Jewett, D. Stelter, J. Lambert, S. M. Saladi, O. M. Roscioni, M. Ricci, L. Autin, M. Maritan, S. M. Bashusqeh, T. Keyes, R. T. Dame, J.-E. Shea, G. J. Jensen and D. S. Goodsell, Moltemplate: A Tool for Coarse-Grained Modeling of Complex Biological Matter and Soft Condensed Matter Physics, *J. Mol. Biol.*, 2021, **433**, 166841.

36 A. Stukowski, Visualization and analysis of atomistic simulation data with OVITO–the Open Visualization Tool, *Modell. Simul. Mater. Sci. Eng.*, 2009, **18**, 015012.

37 C. Ashraf, S. Shabnam, A. Jain, Y. Xuan and A. C. T. van Duin, Pyrolysis of binary fuel mixtures at supercritical conditions: a ReaxFF molecular dynamics study, *Fuel*, 2019, **235**, 194–207.

38 S. Campen, J. Green, G. Lamb, D. Atkinson and H. Spikes, On the Increase in Boundary Friction with Sliding Speed, *Tribol. Lett.*, 2012, **48**, 237–248.

39 R. Lu, H. Zhang, Y. Mitsuya, K. Fukuzawa and S. Itoh, Contributions of Mobile and Bonded Molecules to Dynamic Friction of Nanometer-Thick Perfluoropolyether Films Coated on Magnetic Disk Surfaces, *Tribol. Lett.*, 2014, **54**, 237–247.

40 R. Lotfi, A. C. T. van Duin and M. M. Biswas, Molecular Dynamics Simulations of Perfluoropolyether Lubricant Degradation in the Presence of Oxygen, Water, and Oxide Nanoparticles using a ReaxFF Reactive Force Field, *J. Phys. Chem. C*, 2018, **122**, 2684–2695.

41 H. Tani, Y. Shibahara, R. Lu, S. Koganezawa and N. Tagawa, TOF-SIMS analysis of perfluoropolyether lubricant smear transferred from disk surface following laser heating, *Microsyst. Technol.*, 2020, **26**, 79–88.

42 L. Li, P. M. Jones and Y.-T. Hsia, Effect of Chemical Structure and Molecular Weight on High-Temperature Stability of Some Fomblin Z-Type Lubricants, *Tribol. Lett.*, 2004, **16**, 21–27.

43 T. Kuwahara, P. A. Romero, S. Makowski, V. Weihnacht, G. Moras and M. Moseler, Mechano-chemical decomposition of organic friction modifiers with multiple reactive centres induces superlubricity of ta-C, *Nat. Commun.*, 2019, **10**, 151.

44 K. Hayashi, S. Sato, S. Bai, Y. Higuchi, N. Ozawa, T. Shimazaki, K. Adachi, J.-M. Martin and M. Kubo, Fate of methanol molecule sandwiched between hydrogen-terminated diamond-like carbon films by tribochemical reactions: tight-binding quantum chemical molecular dynamics study, *Faraday Discuss.*, 2012, **156**, 137–146.

45 J. Yeon, X. He, A. Martini and S. H. Kim, Mechanochemistry at Solid Surfaces: Polymerization of Adsorbed Molecules by Mechanical Shear at Tribological Interfaces, *ACS Appl. Mater. Interfaces*, 2017, **9**, 3142–3148.

46 K. Ono, Physics of the Sub-Monolayer Lubricant in the Head-Disk Interface, *Lubricants*, 2024, **12**, 117.

47 T. Shu, H. Li, S. Shen, W. Shen and F. Cui, Dynamic Performance of Head–Disk Interface in HAMR Using Molecular Dynamics Simulation Method, *IEEE Trans. Magn.*, 2018, **54**, 1–5.

48 X. Dai, H. Li, S. Shen and S. Wu, Study of Perfluoropolyether Lubricant Consumption and Recovery in Heat Assisted Magnetic Recording Using Molecular Dynamics Simulation Method, *IEEE Trans. Magn.*, 2017, **53**, 1–6.

49 B. Marchon, X. C. Guo, S. Canchi, R. H. Wang, N. Supper, J. Burns, S. Deoras, J. Zhang, A. Yang, N. Bach and Y. Saito, Air Entrapment in Nanometer-Thick Lubricant Films and its Effect on Slider Flying Height in a Hard Disk Drive, *Tribol. Lett.*, 2012, **47**, 349–355.

50 R. Brunner, PhD thesis, UC San Diego, 2009.